

UC San Diego

UC San Diego Previously Published Works

Title

Lung T2* mapping using 3D ultrashort TE with tight intervals δTE

Permalink

<https://escholarship.org/uc/item/9j63g7qm>

Authors

Malis, Vadim
Kassai, Yoshimori
Vucevic, Diana
et al.

Publication Date

2023-06-08




DOI

10.1002/mrm.29756

Peer reviewed

TECHNICAL NOTE

Lung T_2^* mapping using 3D ultrashort TE with tight intervals δTE

Vadim Malis¹  | Yoshimori Kassai² | Diana Vucevic¹ | Won C. Bae^{1,3}  |
Yoshiharu Ohno^{4,5} | Andrew Yen¹ | Mitsue Miyazaki¹ 

¹Department of Radiology, University of California, San Diego, La Jolla, California, USA

²Canon Medical Systems Corp., Otawara, Japan

³Department of Radiology, VA San Diego Healthcare System, San Diego, California, USA

⁴Department of Radiology, School of Medicine, Fujita Health University, Toyoake, Japan

⁵School of Medicine, Joint Research Laboratory of Advanced Medical Imaging, Fujita Health University, Toyoake, Aichi Japan

Correspondence

Mitsue Miyazaki, Department of Radiology, University of California, San Diego, 9427 Health Sciences Drive, La Jolla, CA 92093-0997, USA.
Email: mimiyazaki@health.ucsd.edu

Funding information

Canon Medical Systems Corp., JAPAN, Grant/Award Number: 35938; National Institutes of Health, Grant/Award Number: R01HL154092

Purpose: To develop 3D ultrashort-TE (UTE) sequences with tight TE intervals (δTE), allowing for accurate T_2^* mapping of lungs under free breathing.

Methods: We have implemented a four-echo UTE sequence with δTE (< 0.5 ms). A Monte-Carlo simulation was performed to identify an optimal number of echoes that would result in a significant improvement in the accuracy of the T_2^* fit within an acceptable scan time. A validation study was conducted on a phantom with known short T_2^* values (< 5 ms). The scanning protocol included a combination of a standard multi-echo UTE with six echoes (2.2-ms intervals) and a new four-echo UTE ($TE < 2$ ms) with tight TE intervals δTE . The human imaging was performed at 3 T on 6 adult volunteers. T_2^* mapping was performed with mono-exponential and bi-exponential models.

Results: The simulation for the proposed 10-echo acquisition predicted over 2-fold improvement in the accuracy of estimating the short T_2^* compared with the regular six-echo acquisition. In the phantom study, the T_2^* was measured up to three times more accurately compared with standard six-echo UTE. In human lungs, T_2^* maps were successfully obtained from 10 echoes, yielding average values $T_2^* = 1.62 \pm 0.48$ ms for mono-exponential and $T_{2s}^* = 1.00 \pm 0.53$ ms for bi-exponential models.

Conclusion: A UTE sequence using δTE was implemented and validated on short T_2^* phantoms. The sequence was successfully applied for lung imaging; the bi-exponential signal model fit for human lung imaging may provide valuable insights into the diseased human lungs.

KEYWORDS

bi-exponential model, lung T_2^* , short and long T_2 components, ultrashort TE (UTE)

1 | INTRODUCTION

MRI is a valuable imaging tool for the evaluation of lung diseases and abnormalities, providing a detailed and

noninvasive approach to examine lungs and the surrounding structures. However, lung MRI remains challenging for routine clinical needs due to its susceptibility and motion artifacts related to respiration and cardiac

pulsations. Additionally, lung parenchyma has intrinsically short T_2^* properties and low proton density, making it extremely difficult to image using conventional MR techniques. In general, lung MRI requires breath-holding, electrocardiographic gating (ECG), and/or respiratory control. Unlike conventional MRI sequences, Ultrashort TE (UTE) imaging with a TE of less than 0.1 ms allows capturing signals from the anatomies with short T_2^* .¹ A multi-echo UTE sequence can be used to generate a set of images with different TEs, allowing for T_2^* mapping.² In medical diagnosis, T_2^* mapping can be used for detecting water content and the presence of pathological tissue as well as for monitoring a variety of diseases and conditions.³⁻⁵ Lung T_2^* maps have been previously reported at 1.5 T using conventional gradient-echo (GRE) sequences.^{6,7} At 3 T, the signal from lung parenchyma decays even faster, making it impractical to use the conventional GRE due to the lower SNR. More recent studies at 3 T used multi-echo 2D-UTE⁸ and dual-echo 3D-UTE⁹ for humans and a multiscan 3D-UTE on rodents¹⁰ with T_2^* maps derived using a mono-exponential signal decay model. Yet, several studies on the lung¹¹ and musculoskeletal systems have demonstrated the advantages of a bi-exponential model fit,^{12,13} such as the ability to distinguish between the fractions of restricted and free water. The accuracy of the bi-exponential mapping depends on the number of acquired echoes and the spacing between them. This poses a challenge for the multi-echo UTE, in which shorter echo intervals are restricted due to the dB/dt hardware limitations. Acquiring these shorter TEs by shifting the first echo several times requires multiple separate acquisitions. To overcome this constraint, we have implemented a free-breathing 3D-UTE with tight TE intervals (δTE), which allows us to collect echoes between the first TE and the following TEs for closely spaced short TE (< 2 ms) echoes within a single scan. The purpose of this study was to validate our novel 3D-UTE sequence with δTE on a phantom with known short T_2^* values and to apply it in in vivo human lung imaging. This innovative approach allows for short TE echoes in tight δTE intervals ($TE_1 = 0.096$ ms $< \delta TE < TE_2 = 2.2$ ms), providing supplementary data to improve the accuracy of T_2^* mapping of the lung. Ultimately this could improve clinical diagnosis and treatment of lung disease.

2 | METHODS

2.1 | Study design

The study was approved by the Institutional Review Board of the University of California, San Diego (200335). We

obtained written informed consent from all study participants. Both phantom and in vivo human lung imaging experiments were performed.

2.2 | Sequence design

Schematic pulse sequence diagrams for multi-echo UTE and UTE with tight echo time intervals δTE are shown in Figure 1A,B, respectively. The variable TE UTE sequence was implemented on a clinical 3T scanner (Vantage Galan 3 T, version 7; Canon Medical Systems Corp., Japan). The position of the first echo in the UTE with δTE (Figure 1B) can be varied in small increments between the first and second echoes of multi-echo UTE. In the diagram, the first echo is shown shifted by δTE , and a possible n th shift $n \cdot \delta TE$ is shown with dashed gradients and thinner line echo. The gating and segmentation scheme is shown in Figure 1C. The lines are acquired in segments (dashed box): The higher the number of segments (N_R), the smaller the acquisition window is. The segment itself is split into parts (green boxes), depending on the number of spectral adiabatic inversion-recovery (SPAIR) pulses per segment (N_{fatsat}). For each SPAIR pulse, n radial lines are acquired. A total of 8160 radial lines are acquired per slab, per TE (N_{total}); this can be written as $N_{total} = N_R \cdot N_{fatsat} \cdot n$, where the number of segments was $N_R = 48$, the number of SPAIR pulses per segment was $N_{fatsat} = 5$, and the number of lines per SPAIR pulse was $n = 34$.

2.3 | Simulation

Commonly used monocomponent and bicomponent models for signal decays $S(t)$ are given by Eqs. (1) and (2), respectively:

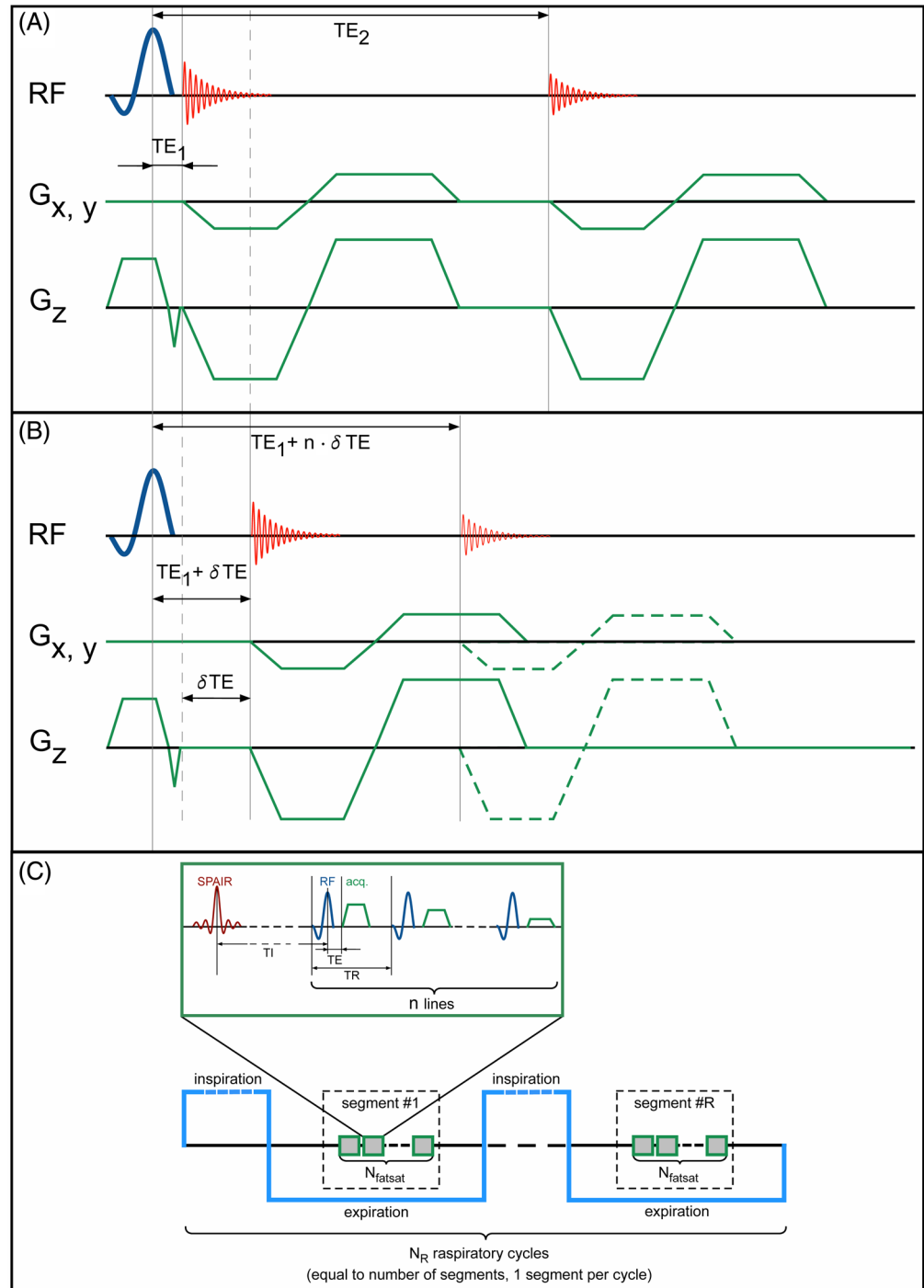
$$S(t) = S(0) \cdot \exp(-t/T_2^*) + S' \quad (1)$$

$$S(t) = S_s(0) \cdot \exp(-t/T_{2s}^*) + S_l(0) \cdot \exp(-t/T_{2l}^*) + S' \quad (2)$$

A mono-exponential model has two parameters: T_2^* and $S(t=0)$. The bi-exponential model has four: $T_{2s,l}^*$ for short (restricted) and long (free) T_2^* and signal coefficients $S_{s,l}(0)$ of short and long T_2^* , respectively. Signal fractions are calculated from the signal coefficients as $f_s = S_s/(S_s + S_l)$ for short and $f_l = S_l/(S_s + S_l)$ for long components. Both models also incorporate a noise term S' .

Monte-Carlo simulation was performed to estimate the accuracy of fits when acquiring additional echoes. A set of 250 000 signals was generated according to Eq. 2 with the combination of the parameters given in Table S1A.

FIGURE 1 (A,B) Schematic pulse sequence diagrams of multi-echo ultrashort TE (UTE) and UTE with tight echo time intervals (δTE). The position of the first echo in the UTE with δTE can be varied for the different segments within a single scan. In the diagram, the first echo is shown shifted by δTE , and a possible n th shift $n \cdot \delta TE$ is shown with dashed gradients and thinner line echo. (C) Schematic demonstrating the sequence segmentation and gating. The lines are acquired in segments (dashed box): The higher the number of segments (NR), the smaller the acquisition window is. The segment itself is split into parts (green boxes), depending on the number of spectral adiabatic inversion-recovery (SPAIR) pulses per segment (N_{fatsat}). For each SPAIR pulse, n radial lines are acquired. A total of 8160 radial lines are acquired per slab, per TE (N_{total}); this can be written as $N_{total} = NR \cdot N_{fatsat} \cdot n$.



White Gaussian noise with variable SNR (TE dependent, estimated from the acquired lung images and varying from $SNR_{TE1} = 30$ to $SNR_{TE10} = 12$) was independently generated 1000 times for each combination of the parameters ($n = 250$). The sampling time schemes for 6 to 10, 15, 20, and 25 echoes are given in Table S1A. The range of the parameters is provided in Table S1B, and T_{2s}^* values (< 2.5 ms) were selected based on previously reported T_2^*

values in lung obtained from a mono-exponential fit.^{8,14} The T_{21}^* range was chosen such that the minimum value is at least 4 times higher¹² than the maximum T_{2s}^* (2.5 ms), and the fractions were chosen to span the range from 10% to 90%.

The percent error between predefined and measured parameters was computed as a measure of the accuracy for the given sampling scheme.

2.4 | Phantom study

The study was carried out on a phantom (Model 450; Calimetrix, Madison, WI, USA) featuring five short T_2^* inserts with relaxation times close to those expected in lungs (4.44/3.62/2.27/1.89/1.05 ms, all less than 5 ms). The scanning protocol included (i) a multi-echo UTE with six $TEs = 0.096/2.3/4.5/6.7/8.9/11.1$ ms, $TR = 14.7$ ms, number of excitations (NEX) = 1, flip angle (FA) = 4° , FOV = 25×25 cm in the axial orientation, and matrix size = 256×256 ; additional echoes were acquired with (ii) UTE with δTE , four $TEs = 0.34/0.74/1.14/1.54$ ms ($\delta TE = 0.4$ ms), and same TR (14.7 ms). A total of 8160 radial lines were acquired for each TE in both scans (multi-echo UTE and UTE with δTE), resulting in a scan time of 9 min. Data from a multi-echo UTE (six echoes) and combined 10 echoes (six echoes from multi-echo UTE and four echoes from UTE with tight echo time intervals δTE) were fitted using a mono-exponential model.

2.5 | Human study

The human study included 6 healthy adult volunteers (34 ± 10 years, ranging from 22 to 50 years old) scanned with informed consent. Two individuals previously had coronavirus disease 2019 (COVID-19) but recovered a few months before participating in this study. All images were acquired using 16-channel body and 16-channel spine SPEEDER coils. The scanning protocol included the following scans: (a) 3D UTE without fat suppression ($TE/TR = 96 \mu s/3.7$ ms, NEX = 1, FA = 5°); (b) multi-echo UTE (six $TEs = 0.096/2.3/4.5/6.7/8.9/11.1$ ms, with fat suppression: The total of 8160 radial lines was divided into 48 segments, resulting in 170 lines per segment; the 170 UTE lines were further segmented to have five SPAIR pulses per each of the 48 segments, resulting in one SPAIR pulse per 34 UTE lines [Figure 1C], $TR = 14.7$ ms, NEX = 1, and FA = 4°); and (c) UTE with δTE (four $TEs = 0.34/0.74/1.14/1.54$ ms, $TR = 14.7$ ms) and same 48 segments with five SPAIR fat suppression pulses in each. All study scans were acquired with the respiratory bellows during the expiratory phase of the cycle and shared the same geometric parameters: coronal orientation, FOV = 40×20 cm, and matrix size = 256×256 . Total scan time varied from 16 up to 20 min, depending on the respiratory rate. Images from the scan were used for an automated lung volume segmentation using a set of morphological operations, finding two largest areas with a low signal at each slice, dropping voxels with less than 13 nearest neighbor connections, and the resultant lung surface was smoothed with a 3D Gaussian kernel.¹⁵

2.6 | T_2^* mapping using multi-echo 3D UTE

For a phantom study, two time-dependent signal curves (six echoes only from the multi-echo UTE and 10 echoes from both multi-echo UTE [six echoes] and UTE with δTE [four echoes]) were fitted to the mono-exponential model (Eq. [1]) using the least-squares method. The precision of the calculated T_2^* was evaluated by determining the percentage error in comparison with established phantom T_2^* values. The lung mapping process used mono-exponential and bi-exponential models (Eqs. [1] and [2]), but limited the bicomponent analysis to only those voxels that met the condition of $4 \cdot T_{2s}^* < T_{2l}^*$.¹²

Simulation study and image processing were implemented in *MATLAB* (R2022b; MathWorks, Natick, MA, USA) using curve fitting and parallel processing toolboxes.

3 | RESULTS

3.1 | Simulation

The results of a Monte Carlo simulation are demonstrated in Figure 2C. The bar chart compares the accuracy of the parameters ($T_{2s,l}^*$ and $f_{s,l}$) estimated from the bicomponent model fit for the multi-echo acquisitions with 6 to 10, 15, 20, and 25 echoes. The results demonstrate a noticeable decrease in error for T_{2s}^* (compared with true value) from 56% error (6 echoes) to 26% error (10 echoes). However, the precision of T_{2s}^* does not improve much when increasing to 15, 20, and 25 echoes (24% error for 25 echoes). Accuracy for T_{2l}^* ranges from a 47% error for 6 echoes to 35% for the 25-echo acquisition (10 echoes have a 39% error). Errors for short f_s and long f_l fractions turned out to be below 25% for all the acquisition schemes and decreased gradually with more echoes added.

3.2 | Phantom study

Axial image of T_2^* phantom with colored regions of interest (ROIs) corresponding to the five short T_2^* inserts is shown in Figure 3A. Figure 3B–K demonstrates all 10 echoes collected with multi-echo UTE (B,G–K) and UTE with δTE (C–F). Note the significant drops in signal intensities for ROIs 3–5 between $TE = 0.096$ (B) and $TE = 2.3$ ms (G). These ROIs (3–5) are consecutive TE images between the first and second echoes of multi-echo UTE. The signals in (C)–(F) from UTE with δTE provide a smooth signal transition of a gradual decrease, as compared with multi-echo UTE signals between (B) and (G), which may allow a better estimation of T_2^* relaxation times. Comparisons between

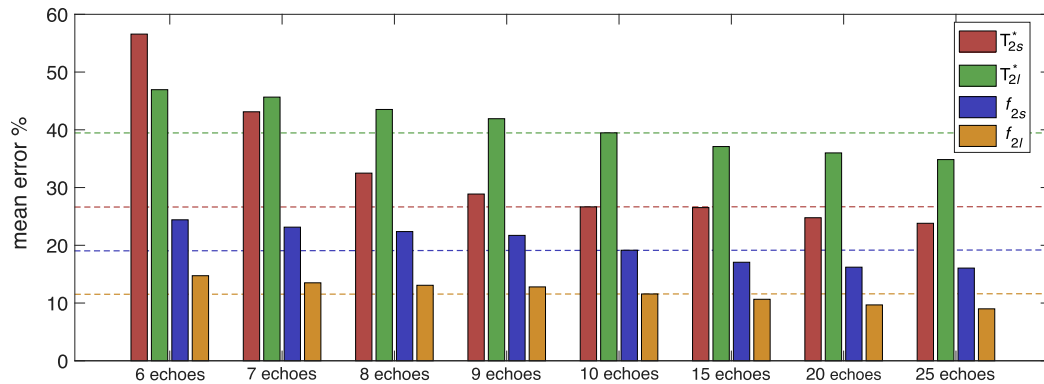


FIGURE 2 Grouped bar chart with mean error percentage demonstrates the results of the Monte-Carlo simulation comparing the accuracy of the bicomponent model fit for the acquisitions with 6, 7, 8, 9, 10, 15, 20, and 25 echoes. The colored dashed lines in the background provide reference to the mean errors for the 10-echo fit. Note the large increase in accuracy for T_{2s}^* component (red) between the 6-echo and 10-echo acquisition, whereas the increase between the 10-echo and 25-echo acquisition is much smaller and thus negligible. Accuracy for T_{2l}^* (green) ranges from 47% error for the 6-echo acquisition to 35% for the 25-echo acquisition (10 echoes has 39% error). Errors for short f_s (blue) and long f_l (orange) fractions were below 25% for all the acquisitions schemes, gradually decreasing with more echoes added.

6-echo and 10-echo mono-exponential fits for five phantom inserts are shown in Figure 3L–P. Six-echo fit curves are given in blue, while 10-echo fit curves are given in red. Discrepancies or mismatches in the fits are noticeable with $T_2^* = 1.89$ in (D) and 2.27 ms in (C). Visually, the six-echo fit appears to provide a precise fit. However, the signal decay between the first and second echoes of the multi-echo sequence (six echoes, blue circles) is substantially rapid in all the plots (L–P) in Figure 3. Note that T_2^* measures using 10 echoes from UTE and UTE with δTE show closer values to known T_2^* values of the five inserts in the Figure 3. Due to rapid signal decay and as a result lower SNR for all echoes with $TE > 2$ ms, the fits obtained using only six echoes consistently underestimated T_2^* for all phantom inserts. Figure 3Q shows the bar chart of the percent error between true and estimated T_2^* values. High percent errors for T_2^* estimated from six echoes compared with percent errors from 10 echoes are seen for inserts with $T_2^* = 1.06$ ms and 1.89 ms, which are closest to those anticipated for human lungs, reported previously.^{8,14}

3.3 | Human lung imaging

Figure 4 shows renderings of the extracted lung volume front (B) and back (C) coronal views. High contrast in non-fat-suppressed UTE image volume between lung tissue and all the surrounding anatomies allowed for a simple but robust segmentation. The segmented lung volumes were then used to calculate mean T_2^* from the mono-exponential model, and $T_{2s,l}^*$ and their corresponding fractions $f_{s,l}$ from bi-component model. A single slice in coronal orientation with estimated lung T_2^* color maps in a healthy adult volunteer is shown in Figure 4D–I:

T_2^* from mono-exponential fit (D), bi-exponential model fit colormaps with short T_{2s}^* (E), and long T_{2l}^* (F). Highlighted with green are the boundaries of the segmented lung volume (Figure 4B,C), with the overlaid red voxels satisfying the condition for mono-component only (Figure 4G) and the fractions of short and long T_2^* from the bi-exponential fits (Figure 4H,I), respectively. The colormaps appeared to be homogeneous with average T_2^* values of 1.62 ± 0.48 ms for mono-exponential fit, which is in good agreement with the values reported in prior studies.^{8,14} Mapping from the bi-exponential model yielded a slightly more homogenous colormap for short T_{2s}^* with average values of 1.00 ± 0.53 ms, more than 50% lower than from the mono-exponential fit. Typical monocomponent and bicomponent fit curves in the lung parenchyma ROI are shown in Figure S4. Per-subject average values for T_2^* and T_{2s}^* are provided in Table S2 and are presented as a bar chart with SD error bars in Figure S1. Single-slice colormaps of T_2^* (from mono-exponential model) and T_{2s}^* (from bi-exponential model) are shown in Figures S2 and S3. On average, over 68% of the lung volume showed two components, with long T_{2l}^* being 123.89 ± 25.88 ms. The fraction of long component f_l was found to be $27.9\% \pm 11.3\%$ (consequently, short fraction $f_s = 72.1\% \pm 11.3\%$). Figure 5 demonstrates the colormaps of long T_{2l}^* fraction f_l for a single coronal slice, with the largest cross-sectional area for all the volunteers participated in the study.

4 | DISCUSSION

The non-radiation nature of MRI has made it an appealing option for pulmonary imaging, as an alternative to

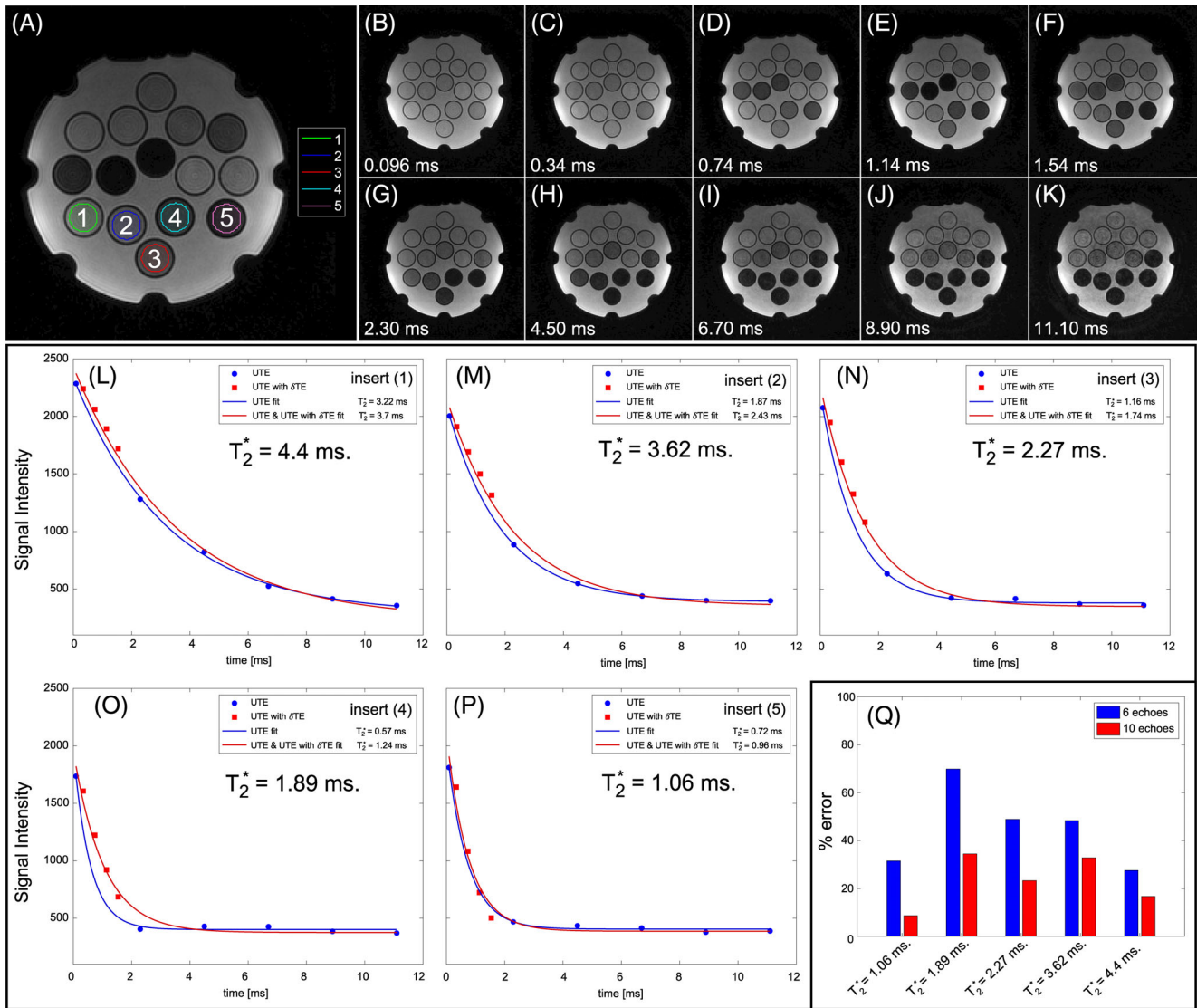


FIGURE 3 (A) Axial image of T_2^* phantom with overlaid colored regions of interest (ROIs) corresponding to the five short T_2^* inserts. (B–K) All 10 echoes collected with multi-echo ultrashort TE (UTE) (B,G–K, six echoes) and UTE with tight echo time intervals (δTE) (C–F, four echoes). Note the significant decreases in signal intensities for ROIs 3–5 between TE = 0.096 ms (B) and TE = 2.3 ms (G). (L–P) Comparisons between the 6-echo and 10-echo mono-exponential model fits for the five phantom inserts marked on (A). Six echoes from multi-echo UTE are plotted in blue circles with the corresponding mono-exponential fit curves (also blue), whereas the 10-echo (six echoes from multi-echo UTE combined with four echoes from UTE with tight echo time intervals [δTE] intervals [red squares]) with mono-exponential fit curves are given in red. Discrepancy of the fits is best noticeable for inserts with T_2^* of 2.27 and 1.89 ms. A stacked bar chart demonstrates the error percentage between the true and estimated T_2^* values (F) for the same five phantom inserts as in (L)–(E).

CT and X-ray. However, because of low proton density, short T_2^* of the lung parenchyma, and respiratory motion, it is a challenging task. While regular GRE sequences with a Cartesian sampling scheme operate with TE ≥ 1 ms,⁷ radial 3D UTE permits TE as low as 0.1 ms (or 100 μ s). The use of a UTE makes it possible to measure a substantial signal from the lung parenchyma with an ultrashort T_2 component and allows for accurate T_2^* mapping.¹⁶ Radial 3D UTE acquires data from the center of k -space with ramp sampling in the radial direction, without using phase and slice encoding. This approach provides intrinsic

motion compensation because of oversampling of the center of k -space. With appropriate segmentation, the radial lines are collected under free breathing using respiratory bellows.

The main limitation of multi-echo 3D UTE that affects the precision of T_2^* mapping is its inability to capture closely spaced echoes within a single acquisition. The acquisition scheme introduced in UTE with δTE overcomes this limitation, providing additional echoes between the first (shortest) and second echoes in conventional multi-echo 3D UTE. Nonetheless, the enhanced

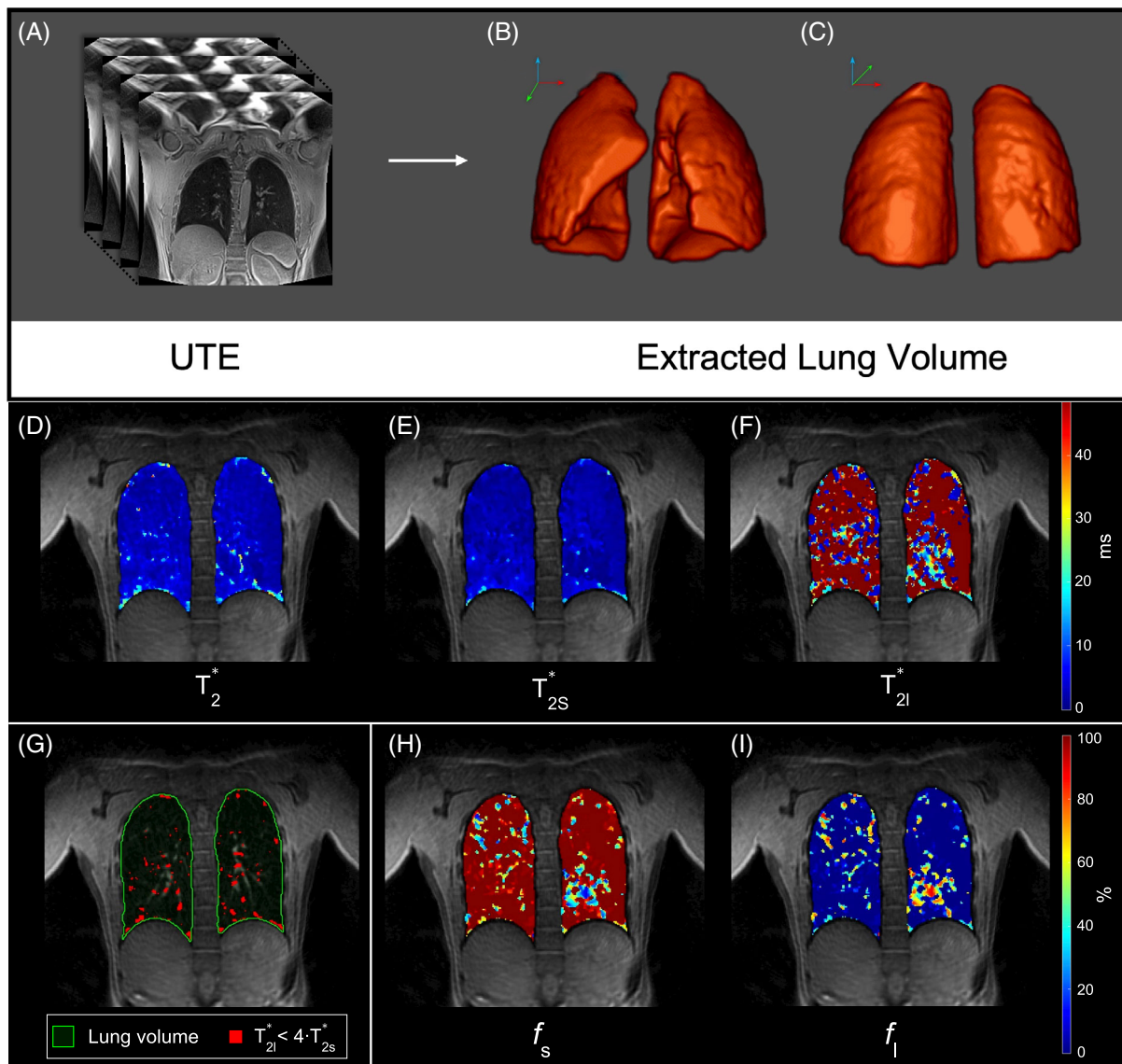


FIGURE 4 (A) Top: Non-fat-suppressed ultrashort TE (UTE) image volume and extracted lung volume renderings: front (B) and back (C) coronal views. Bottom: Estimated T_2^* lung colormaps for a healthy adult volunteer. (D) T_2^* from mono-exponential fit, bi-exponential model fit colormaps with short T_{2s}^* (E), and long T_{2l}^* (F). (G–I) Highlighted in green are the boundaries of the segmented lung volume with the overlaid red voxels satisfying condition for mono-exponential fit only (G) and the fractions of short and long T_2^* , respectively (H,I).

accuracy of T_2^* mapping using additional δTE echoes comes with a trade-off of longer scan times. Therefore, it is crucial to determine an optimal balance between scan time and the number of additional echoes to achieve the desired accuracy. The 10-echo scheme proposed in this study is based on the simulation results and was tested on a short T_2^* phantom.

UTE images with high temporal TE resolution were previously collected ex vivo for various specimens and cadaveric tissues in tendon and knee¹⁷ as well as in rodent lungs under anesthesia.^{10,18} The current study shows the feasibility of T_2^* mapping using UTE imaging with high

temporal TE resolution δTE on in vivo human lungs in 3D. The T_2^* values obtained in this study with the mono-exponential model are in good agreement with earlier findings obtained through single-slice UTE⁸ and 3D UTE obtained in four separate acquisitions.¹⁴

The application of a single exponential model to quantify T_2^* values in lung parenchyma proved to be a valuable tool in the evaluation of pulmonary functional loss.¹⁹ However, the accuracy of the single-compartment model in describing signal evolution may be limited, particularly when the fractions of the compartments with different T_2^* values are comparable. The bi-exponential model

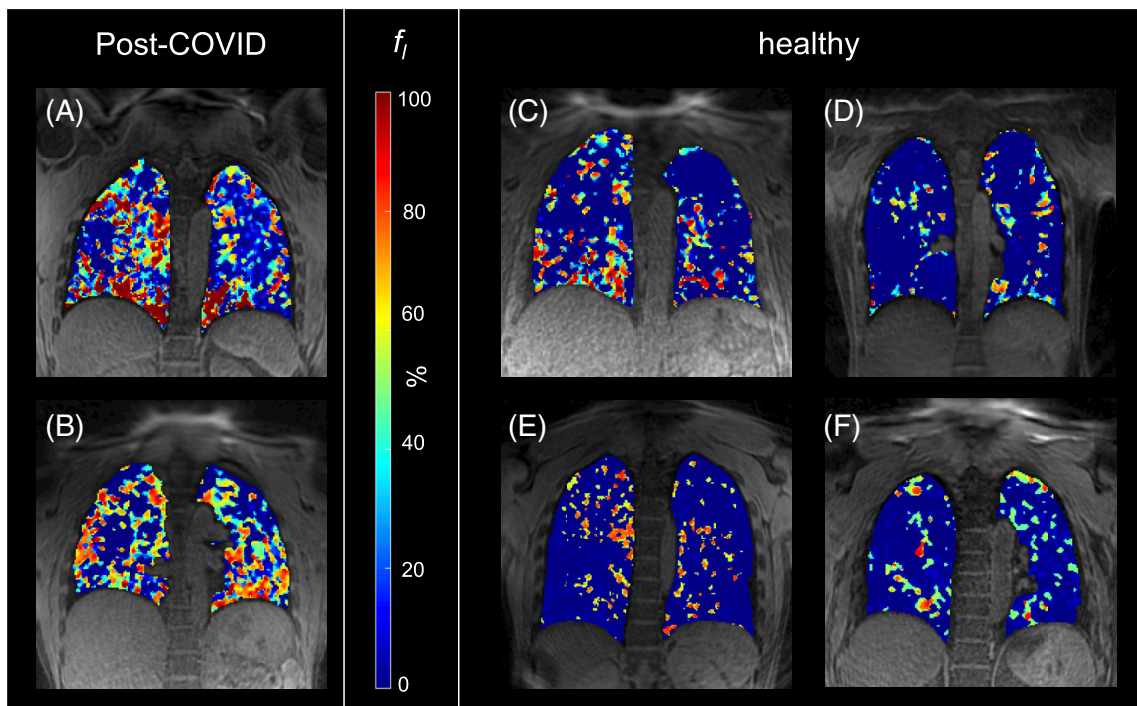


FIGURE 5 Long T_2^* fraction f_1 colormaps for a single coronal slice with the largest cross-sectional area for all the volunteers participating in the study. Post-coronavirus disease (COVID) subjects are shown on the left in (A,B), and healthy subjects on the right (C–F). Note the higher long T_2^* fraction f_1 values of the post-COVID participants.

can be useful in distinguishing the contributions from lung parenchyma with blood and mucus distribution, and consequently increase the accuracy of T_{2s}^* measurement.¹¹ In this study, on average, almost 70% of lung volume demonstrated the presence of a two-component signal. Short and long relaxation times derived from the bi-component model were consistent across subjects; however, a fraction of short/long T_2^* components varied across the subjects, resulting in a large SD (11.3%). Two volunteers had a much higher fraction of long T_2^* , as compared with others (Figure 5). Our hypothesis is that the lung parenchyma signal in these subjects (both recently recovered from COVID-19, $f_1 = 34$ and 39%) might be contaminated with the long T_2^* component like mucus in the bronchioles and alveoli. Several studies have demonstrated mucus accumulation in the lungs of COVID-19 patients.^{20,21} A recent study using UTE imaging on COVID patients revealed that visual examination can be a viable diagnostic tool alternative to CT.²² Our bicomponent T_2^* mapping using UTE with δTE may provide an additional quantitative lung biomarker by long and short T_2^* components to investigate long COVID, emphysema, and lung cancers.

With regard to the automated lung volume segmentation used in this study, it is important to note that all volunteers were healthy individuals without any lung pathology

or injury. However, for patients with scarring or atelectasis, manual correction may be required.

5 | CONCLUSIONS

The UTE sequence with δTE was successfully implemented and tested on the short T_2^* phantom and human lung imaging by combining with the conventional multi-echo UTE. Based on our findings, we were able to achieve greater precision in T_2^* mapping for both phantom and human lung imaging. The bicomponent model fit has proven to be a valuable tool for obtaining quantitative metrics of lung parenchyma. In future, we will investigate our bicomponent T_2^* mapping method in patients with pulmonary disease.

ACKNOWLEDGMENTS

The authors thank Dr. Andy Wheaton for the valuable advice on the sequence implementation.

FUNDING INFORMATION

This work was supported by a National Institutes of Health grant R01HL154092 (M.M.) and a research grant from Canon Medical Systems Corp., JAPAN (35938).


CONFLICT OF INTEREST

Part of these results will be presented at the ISMRM 2023. Mr. Yoshimori Kassai is an employee of Canon Medical Systems Corp., Japan.

ORCID

Vadim Malis  <https://orcid.org/0000-0002-0426-1457>

Won C. Bae  <https://orcid.org/0000-0003-2616-0339>

Mitsue Miyazaki  <https://orcid.org/0000-0002-5690-694X>

REFERENCES

- Robson MD, Gatehouse PD, Bydder M, Bydder GM. Magnetic resonance: an Introduction to ultrashort TE (UTE) imaging. *J Comput Assist Tomogr.* 2003;27:825-846. doi:10.1097/00004728-200311000-00001
- Du J, Takahashi AM, Shimakawa A, Brittain JH, Bydder M, Bydder GM. Multiecho ultrashort TE (UTE) imaging and T2* mapping of knee cartilage. In: *Proceedings of the 14th Annual Meeting of ISMRM*, Seattle, Washington, USA 2006 Abstract #57.
- Westwood M, Anderson LJ, Firmin DN, et al. A single breath-hold multiecho T2* cardiovascular magnetic resonance technique for diagnosis of myocardial iron overload. *J Magn Reson Imaging.* 2003;18:33-39. doi:10.1002/jmri.10332
- Bittersohl B, Kircher J, Miese FR, et al. T2* mapping and delayed gadolinium-enhanced magnetic resonance imaging in cartilage (dGEMRIC) of humeral articular cartilage—a histologically controlled study. *J Shoulder Elbow Surg.* 2015;24:1644-1652. doi:10.1016/j.jse.2015.03.016
- He T, Gatehouse PD, Smith GC, Mohiaddin RH, Pennell DJ, Firmin DN. Myocardial T measurements in iron-overloaded thalassemia: an in vivo study to investigate optimal methods of quantification. *Magn Reson Med.* 2008;60:1082-1089. doi:10.1002/mrm.21744
- Stock KW, Chen Q, Hatabu H, Edelman RR. Magnetic resonance T2* measurements of the normal human lung in vivo with ultra-short echo times. *Magn Reson Imaging.* 1999;17:997-1000. doi:10.1016/s0730-725x(99)00047-8
- Theilmann RJ, Arai TJ, Samiee A, et al. Quantitative MRI measurement of lung density must account for the change in T2* with lung inflation. *J Magn Reson Imaging.* 2009;30:527-534. doi:10.1002/jmri.21866
- Yu J, Xue Y, Song HK. Comparison of lung T2* during free-breathing at 1.5 T and 3.0 T with ultrashort echo time imaging. *Magn Reson Med.* 2011;66:248-254. doi:10.1002/mrm.22829
- Gai ND, Malayeri AA, Bluemke DA. Three-dimensional T1 and T2* mapping of human lung parenchyma using interleaved saturation recovery with dual echo ultrashort echo time imaging (ITSR-DUTE). *J Magn Reson Imaging.* 2017;45:1097-1104. doi:10.1002/jmri.25487
- Takahashi M, Togao O, Obara M, et al. Ultra-short echo time (UTE) MR imaging of the lung: comparison between normal and emphysematous lungs in mutant mice. *J Magn Reson Imaging.* 2010;32:326-333. doi:10.1002/jmri.22267
- Lu A, Zhou X, Miyazaki M, Yui M, Umeda M, Ohno Y. Investigation of the multiple T2* compartments in lung parenchyma using a 3D multi-echo radial sequence. In: *Proceedings of the 24th Annual Meeting ISMRM*, Singapore 2016 Abstract #1611.
- Juras V, Apprich S, Szomolanyi P, Bieri O, Deligianni X, Trattig S. Bi-exponential T2* analysis of healthy and diseased Achilles tendons: an in vivo preliminary magnetic resonance study and correlation with clinical score. *Eur Radiol.* 2013;23:2814-2822. doi:10.1007/s00330-013-2897-8
- Diaz E, Chung CB, Bae WC, et al. Ultrashort echo time spectroscopic imaging (UTESI): an efficient method for quantifying bound and free water. *NMR Biomed.* 2012;25:161-168. doi:10.1002/nbm.1728
- Ohno Y, Koyama H, Yoshikawa T, et al. T2* measurements of 3-T MRI with ultrashort TEs: capabilities of pulmonary function assessment and clinical stage classification in smokers. *Am J Roentgenol.* 2011;197:W279-W285. doi:10.2214/ajr.10.5350
- Perona P, Malik J. Scale-space and edge detection using anisotropic diffusion. *IEEE T Pattern Anal.* 1990;12:629-639. doi:10.1109/34.56205
- Malis V, Bae W, Yamamoto A, et al. Free-breathing 3D MRI: T2*, inspiration/expiration lung volume, and pulmonary vasculature. In: *Proceedings of the 30th Annual Meeting of ISMRM 2021 Abstract #3233*. Virtual.
- Ma YJ, Chang EY, Bydder GM, Du J. Can ultrashort-TE (UTE) MRI sequences on a 3-T clinical scanner detect signal directly from collagen protons: freeze-dry and D2 O exchange studies of cortical bone and Achilles tendon specimens. *NMR Biomed.* 2016;29:912-917. doi:10.1002/nbm.3547
- Olsson LE, Hockings PD. In vivo measurements of T2 relaxation time of mouse lungs during inspiration and expiration. *Plos One.* 2016;11:e0166879. doi:10.1371/journal.pone.0166879
- Ohno Y, Nishio M, Koyama H, et al. Pulmonary MR imaging with ultra-short TEs: utility for disease severity assessment of connective tissue disease patients. *Eur J Radiol.* 2013;82:1359-1365. doi:10.1016/j.ejrad.2013.02.031
- Dickey BF, Chen J, Peebles RS. Airway mucus dysfunction in COVID-19. *Am J Resp Crit Care.* 2022;206:1304-1306. doi:10.1164/rccm.202207-1306ed
- Kato T, Asakura T, Edwards CE, et al. Prevalence and mechanisms of mucus accumulation in COVID-19 lung disease. *Am J Resp Crit Care.* 2022;206:1336-1352. doi:10.1164/rccm.202111-2606oc
- Fauveau V, Jacobi A, Bernheim A, et al. Performance of spiral UTE-MRI of the lung in post-COVID patients. *Magn Reson Imaging.* 2023;96:135-143. doi:10.1016/j.mri.2022.12.002

SUPPORTING INFORMATION

Additional supporting information may be found in the online version of the article at the publisher's website.

Table S1. a: Range of parameters used for the simulation study. b: List of echo times for different TE samplings.

Table S2. Per subject average values for T₂* and T_{2s}* with the standard deviation.

Figure S1. Bar chart with per subject average values for T₂* (blue) and T_{2s}* (red) with the standard deviation error bars.

Figure S2. T₂* (mono-exponential model) colormaps for a single slice of each subject.

Figure S3. T_{2s}^* (bi-exponential model) colormaps for a single slice of each subject.

Figure S4. Average signal intensity in parenchyma region of interest measured (red) at different TEs and the bi- (green) and mono- (blue) exponential fit curves. Root-mean square errors for the bi- and mono- component fits are 1.05 and 4.34 respectively.

How to cite this article: Malis V, Kassai Y, Vucevic D, et al. Lung T_2 mapping using 3D ultrashort TE with tight intervals δTE . *Magn Reson Med*. 2023;1-10. doi: 10.1002/mrm.29756